A Letters Journal Exploring the Frontiers of Physics

OFFPRINT

Dynamics of the formation of antibubbles

P. G. Kim and H. A. Stone

EPL, **83** (2008) 54001

A Letters Journal Exploring the Frontiers of Physics

September 2008

EPL, **83** (2008) 54001
doi: 10.1209/0295-5075/83/54001

www.epljournal.org

Dynamics of the formation of antibubbles

P. G. Kim and H. A. Stone[(a)]

School of Engineering and Applied Sciences, Harvard University - Cambridge, MA 02138, USA

received 17 June 2008; accepted in final form 10 July 2008
published online 25 July 2008

PACS 47.55.db – Drop and bubble formation
PACS 82.70.Uv – Surfactants, micellar solutions, vesicles, lamellae, amphiphilic systems, (hydrophilic and hydrophobic interactions)
PACS 47.20.Cq – Inviscid instability

Abstract – Antibubbles refer to drops of liquid that are surrounded by a thin gas shell with the whole object immersed within a liquid phase. Although first observed more than 70 years ago, only recently have details of the formation and disappearance of antibubbles been considered. Here we provide an experimental study of the optimal conditions necessary for the formation of antibubbles. In addition, we characterize the dynamics of the collapse of the liquid column, formed from the initial impact of a drop with a liquid bath, which eventually leads to the antibubble.

Introduction. – Numerous processes such as cleaning, inkjet printing, emulsion formation, combustion, and gas-liquid reactors warrant a careful study of the impact of liquids on liquid and solid substrates [1]. In addition, splashing is so common that we take it for granted, but the impact of a liquid or solid on a liquid bath can lead to air entrainment, which produces the underwater sound of rain as well as bubbles that may have long lifetimes if surfactant is present in solution. Aside from the practical applications, the physics of falling (rain) drops has been extensively studied (*e.g.* [2]) and such dynamically changing liquid-air interfaces often cause bubble formation.

Here we focus on antibubbles, which are ephemeral gas-liquid shells consisting of a pocket of liquid enclosed by a thin film of gas, which is itself (usually) surrounded by the same liquid. In a real sense, they are the inverse of an ordinary gas bubble in water, but their appearance is often mistaken for simple air bubbles. Surprisingly, antibubbles can be successfully created in a variety of different liquids, including Belgian beer [3], diesel oil [4], and through coalescence of bubbles in viscous liquids [5]. These unusual objects were first reported in 1932 [6], and the term antibubbles was coined in 1974 [7]. The experimental conditions sufficient for the formation of antibubbles are rather common, though the formation is restricted to a narrow range of parameter space, which has not been characterized. Here, we investigate the optimal conditions for the formation of antibubbles as well as the dynamics behind their formation.

Antibubble formation is reminiscent of blowing soap bubbles in that it also requires a deformation of the surface, but with a liquid instead of air. Antibubbles are observed when drops, or more accurately liquid columns, of surfactant solution are gently injected into a bath of the same solution. As the liquid impacts the surface, an air film is entrained between the two liquids, which effectively creates a nonwetting situation (fig. 1, frames a–c, imaged at 500 fps). The liquid then elongates and finally pinches off from the surface to form a liquid pocket surrounded by a shell of gas: an antibubble (fig. 1, frames d–h). We find that for an aperture of radius 2.2 mm and an aqueous system with surface tension $\gamma = 26\,\mathrm{mN/m}$, then the drop height and initial velocity of the liquid column needed for the formation of antibubbles should be, respectively, in the range 8–18 mm and less than 24 cm/s.

The air film is a crucial and defining element of an antibubble. The compressibility of the air in the thin film contributes to its stability and the existence of a critical hydrostatic pressure, above which the film ruptures, has been reported [8]. Moreover, the gravitational thinning of the air film and its effect on the lifetime of antibubbles have been discussed [9]; we consider aspects of the drainage below. Even though the "death" of antibubbles has been studied [10], little is known about the conditions for their formation. Since future study of these objects and possible applications require that antibubbles be produced controllably, we report a detailed study of the dynamics

[(a)] E-mail: has@seas.harvard.edu

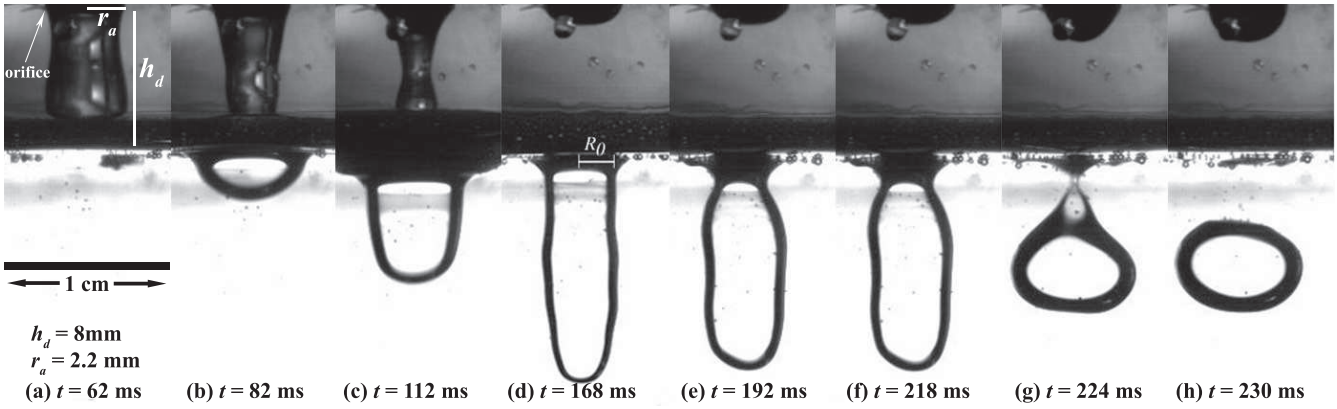

Fig. 1: Formation of an antibubble. To examine antibubble formation closely, these particular frames were captured at 500 fps. The black boundary is the entrained air film that forms the antibubble. The black bar in frame (a) indicates 1 cm.

of formation. We are able to rationalize several aspects of the optimal window in parameter space for creating antibubbles.

Experimental details. –

Production of antibubbles. Antibubbles were produced by injecting drop by drop a solution of dishwashing soap (volume fraction 0.1% of Dawn$^{\text{TM}}$ Ultra with tap water) into the same solution; soap solutions that are too dilute do not readily form antibubbles. The liquid was released from a fall height h_d. This solution is above the critical micellar concentration (CMC) at which surfactant molecules start to aggregate in the solution and the surface tension was $\gamma = 26\,\text{mN/m}$ (measured with a pendant-drop method). Our experiments were most consistent when the solution was left overnight before use. To allow for continuous production of antibubbles, we performed experiments in a plexiglass cell ($30.5 \times 30.5 \times 35\,\text{cm}^3$) with an open top and a hole (radius equal to 5 mm) near the top on one side (see fig. 2). The main cell is connected to a smaller closed container that filters any foam that forms. This smaller container in turn is connected to a peristaltic pump (Cole Parmer, Masterflex HV-77919-10) with a single cartridge head (Cole Parmer, 07519-20), which recycles fluid back to the plexiglass cell. Drops with volume about 0.1 ml (radii approximately 3 mm) emerge from the aperture at a frequency of about 6 Hz and velocity v_0 of about 20 cm/s; these speeds were estimated by tracking the position of the leading edge of the liquid column as it approached the bath. The liquid falls a height h_d and impacts the surface of the solution, after which an antibubble may be formed. The setup (fig. 2a) creates a steady state, which allows for efficient clean-up of any foam formed at the liquid-air interface during the experiments; any extra bubbles may impact formation of antibubbles by hindering development of the air film.

Antibubble detection. A trial consists of capturing a continuous production of antibubbles for 30 seconds using

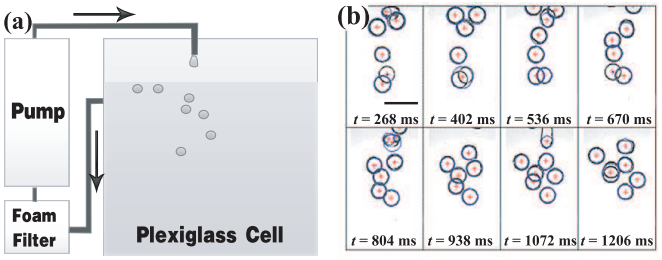

Fig. 2: (a) Sketch of the experiment. The cell is filled with soap solution and the arrows indicate the direction of flow. (b) The detection of antibubbles. The red on-line pluses indicate the centers of the antibubbles detected using the image processing software. The black bar in the first frame indicates 1 cm.

a digital camera operating at 15 fps, and counting the total number of antibubbles produced during this time period using MATLAB image analysis software (fig. 2b). The refraction of light at the liquid-air-liquid interface of an antibubble creates sharp black edges that are detected easily with image processing. Using a gradient-based circular Hough transform [11], the antibubbles center-of-mass coordinates were detected if the radius ranged between 0.8 and 6 mm (the average radius of the antibubble so produced was on average 3 mm). With this method, antibubbles can be detected even if the edges overlap significantly (fig. 2b). Because of the sluggish movement of the antibubbles in the liquid, the bubbles can be tracked with reasonable accuracy, and a tracking program identified each antibubble in one frame with the corresponding antibubble in the next frame. To decrease the noise in the measurement and to not count antibubbles that fail to form, several steps were taken. First, a "successful" antibubble was determined to be one that lasts more than 0.4 s. Second, since antibubbles tend to aggregate on the surface after penetrating a certain depth into the liquid, antibubbles on the surface were not analyzed. Third, to prevent double counting, if antibubbles with similar radii were detected at exactly the same

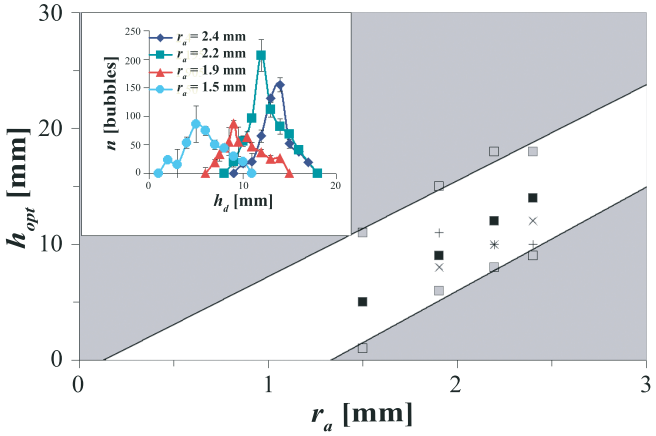

Fig. 3: Phase diagram for antibubble formation. The optimal drop height h_{opt} is reported as a function of the radius of the aperture (r_a) at $v_0 = 20\,\mathrm{cm/s}$; h_{opt} is defined as the fall height h_d that produces the greatest number of antibubbles n in a 30 s interval (inset). The white region of the main graph indicates allowable conditions for formation for one experiment, with the optima identified with black squares and the boundaries by grey squares. 6253 antibubbles in total were tracked for this experiment. Pluses and crosses correspond to optima derived from experiments performed on different days with fresh solutions in which, respectively, 3058 and 1441 antibubbles were tracked. For each point in the inset, three trials were performed and error bars represent mean ± standard deviations.

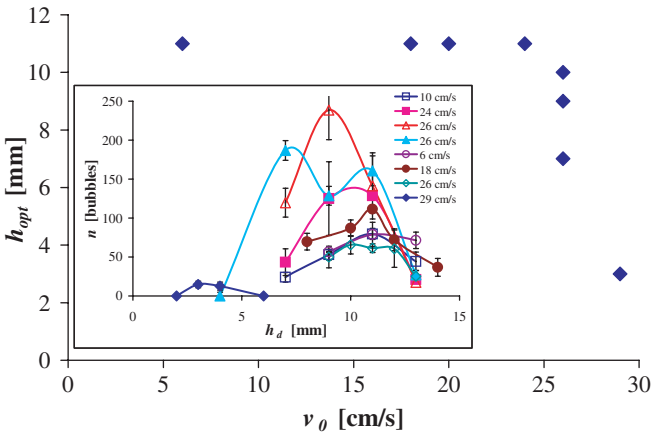

Fig. 4: Optimal drop height as a function of the initial velocity (v_0) of the drop as it leaves the aperture; h_{opt} is defined as the height that produces the greatest number of antibubbles n in a 30 s interval (see inset). Here the orifice radius $r_a = 2.2\,\mathrm{mm}$ and 7239 antibubbles were tracked. For each point in the inset, three trials were performed and error bars represent mean ± standard deviations.

pixel coordinates in a given frame, they were assumed to be one antibubble. Lastly, if the smallest displacement between two sequential frames was greater than 5 mm, the antibubble was assumed to have popped. Manual counting of antibubbles in four trials revealed that the automated image processing program overestimated the actual number of antibubbles by about 6%.

Experimental results. –

Optimal formation. We first investigate the conditions that produce the greatest number of antibubbles by systematically altering the fall height h_d for each aperture radius r_a. To ensure precision, three trials were performed for each h_d ranging from 1 to 20 mm with the same initial velocity v_0 of the liquid leaving the orifice. Using MATLAB image analysis software, we measured v_0 for each radius to ensure that v_0 remained constant.

For each r_a, the number of antibubbles (n) as a function of h_d is approximately normally distributed with a skew towards larger h_d (fig. 3, inset). We refer to the peak of this distribution as the optimal height h_{opt}. In other words, for release heights too small or too large we are unable to form antibubbles. The allowable h_d for forming antibubbles usually fall within ±5 mm of h_{opt}. From these data, we plot the optimal height as a function of the aperture radius, which reveals a linear relationship (fig. 3, black squares, correlation = 0.99). All the above-mentioned data were collected on the same day to control for the reported effect of atmospheric fluctuations [8]. However, data collected on different days (fig. 3, pluses and crosses) had similar ranges.

We also performed experiments changing the initial liquid velocity v_0. Here, we report results for one aperture ($r_a = 2\,\mathrm{mm}$) with which we varied the fall height h_d for each initial liquid velocity v_0. Again, for most v_0, we observe a distribution of the number of bubbles (n) as a function of h_d and again identify an optimal height (fig. 4, inset). For velocities less than approximately 24 cm/s, we observe that the optimal height is constant but for velocities greater than 24 cm/s, we observe a sharp decrease in the optimal height for formation of antibubbles (fig. 4). We note that this transition occurs where the gravitational and kinetic energies are about the same (to within a factor of 2). For larger velocities we observe a rapid decrease in the critical height for the formation of antibubbles. Therefore, the optimal conditions for forming antibubbles for the aperture radii $r_a = 2.2\,\mathrm{mm}$ are roughly $h_{opt} = 11$ mm and $v_0 < 24\,\mathrm{cm/s}$.

These experimental results reveal a narrow window (estimated energy range of about 10 μJ) for optimal formation of antibubbles. In other experimental systems, noncoalescence of drops is primarily caused by factors that delay the drainage of the air in the air film. Some examples of noncoalescence relevant to our experiments include drops on an oscillating bath [12] and temperature differences that maintain noncoalescence between a drop and a nearby substrate [13]. In our experiments with antibubbles, it is most likely that the lubrication form of resistance to flow of air in the narrow gap between the water drop and the liquid bath reduces the drainage rate of the air film [9,14]. We next provide a model that makes this idea clear.

Film lubrication. As the sequence of images in fig. 1 makes clear, the formation of an antibubble requires that i) a liquid cavity is formed while an air film is entrained and ii) the interface behind the falling water column pinches to seal the antibubble before the thin air film in front breaks. We have observed that there is a minimum speed in order to form antibubbles. It is necessary to be able to deform the surface sufficiently to begin to surround the drop (radius R_d) with an air film. This limit corresponds to a critical value of the Weber number $\rho_\ell v^2 R_d/\gamma > 1$, where ρ_ℓ is the density of the liquid and R_d is the radius of the drop. Thus, there is a minimum speed $v_c > (\gamma/(\rho R_d))^{1/2}$. For a 3 mm radius drop, $v_c \approx 10$ cm/s, which is consistent with the velocities observed in fig. 4. It is also consistent with the experimental data that fewer antibubbles form at low h_d, *e.g.* the tails to the left in the distributions of antibubble formation (fig. 3, inset and fig. 4, inset).

Once an air film is formed we consider the lubrication flow of the air through the gap as the water drop falls. The pressure drop Δp along a length ℓ is related to the vertical speed v and the smallest gap dimension $h_0 \ll \ell$ via the equation $\Delta p = O\left(\mu_{air} v \ell^2/h_0^3\right)$. For a water drop of mass m, neglecting for the moment the inertia of the water drop, a vertical force balance requires $mg = O\left(\ell^2 \Delta p\right) = O\left(\mu_{air} v \ell^4/h_0^3\right)$. If the geometry is modeled similar to the squeeze flow between parallel disks of radius R_d, we take $\ell = R_d$ and, as $v = O\left(\mathrm{d}h_0/\mathrm{d}t\right)$, then the time τ to thin the gap scales as $\tau \propto h_0^{-2}$ [9]; a consequence of the "disk" assumption is that the drainage time is controlled by the approach to the smallest gap size (estimated to be 10 nm), which is presumed to involve van der Waals forces [9].

On the other hand, the nearly spherical shape of the drop near the base suggests to us to model the drainage of the air film as the flow between two spheres of nearly equal radius. In this case $\ell \approx \sqrt{h_0 R_d}$ and the hydrodynamic force resisting the motion of the drop is $F = c\mu_{air} R_d^2 v/h_0$, where $v = O\left(\mathrm{d}h_0/\mathrm{d}t\right)$ and $c \approx 6\pi$. Since we wish to describe the formation of an antibubble we also retain the inertia of the drop and so consider the dynamics after a narrow film forms; a vertical force balance on the drop yields

$$\frac{\mathrm{d}^2 h_0}{\mathrm{d}t^2} = -g - \frac{c\mu_{air} R_d^2}{m h_0}\left(\frac{\mathrm{d}h_0}{\mathrm{d}t}\right). \qquad (1)$$

Identifying dimensionless variables $H = h(t)/h(0)$ and $s = t\sqrt{g/h_0(0)}$, integrating eq. (1) once with an initial condition ($t = 0$) that involves the initial impact velocity $V = v(0)/\sqrt{h_0(0) g}$, then we have

$$\frac{\mathrm{d}H}{\mathrm{d}s} = -s - A \ln H - V. \qquad (2)$$

The two dimensionless parameters $A = \frac{c\mu_{air} R_d^2}{m\sqrt{h(0)g}}$ and V characterize, respectively, the drag force from the lubrication flow relative to the inertia of the drop, and the initial downward speed of the drop at the time the thin air gap is formed relative to a fall speed from the height $h(0)$. Typical values are $A = O(10^{-1})$ and $V = O(1\text{–}10)$ (if we take $h(0) \approx 10$ microns). We have solved eq. (2) numerically for some representative values of A and V to illustrate qualitatively the dynamics relevant to antibubble formation. We report results in fig. 5 for $A = 0.1, 0.4$ and 0.6. For the smallest value of A, the drop decelerates only a small amount prior to the gap reaching very small values, at which we assume that nonhydrodynamic effects produce film rupture. This response correlates with the presence of a right tail in the distribution of antibubble formation (fig. 3, inset). For larger values of A, the drop decelerates and there is a significant length of time where an air film of finite thickness is formed, and during which the air film only drains slowly. Over this time scale, if the back of the water column pinches, then an antibubble is formed successfully. To help illustrate the limiting cases that hinder antibubble formation, we show also two sets of images in fig. 5: i) an experiment where there is a finite thickness air film at the front but for which there is a lack of pinching at the back (consistent with the solid curve from the numerical model) and ii) an experiment where rapid drainage occurs at the front (consistent with the dot-dashed curve from the numerical model).

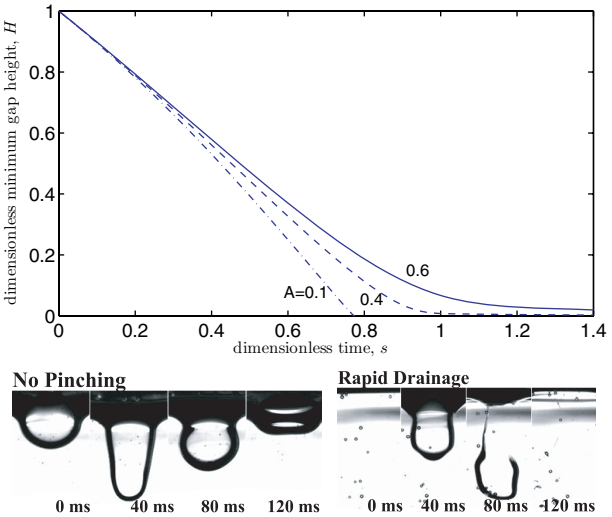

Fig. 5: Lubrication flow model for the change in gap height with time as a liquid drop falls inside a nearly spherical cavity. Equation (2) was solved numerically with $V = 1$ and $A = 0.1$ (dot-dashed curve that shows rapid drainage), 0.4 (dotted curve) and 0.6 (solid curve that shows lack of pinching). The set of images illustrates these two extremes, rapid drainage (dot-dashed curve) and lack of pinching (solid curve), in 40 ms intervals.

There are other conditions that lead to failure to form antibubbles. If the h_d is large enough, Rayleigh-Plateau instability breaks up the liquid jet into multiple drops near the aperture, creates surface disturbances that disrupt the formation of the air film. This phenomenon also limits antibubble formation at high h_d independent of the final impact velocity. Nevertheless, on occasion, we do observe

that small antibubbles form despite breakup of liquid into multiple drops, and perhaps these small antibubbles explain the slightly right-skewed distribution for a given aperture radius (fig. 3, inset).

Antibubble formation is therefore a process complicated by many variables. The trend for the optimal height is puzzling since one would expect that in the model for the viscous reduction in the speed of the drop, once a significant spherical cavity forms, the drops of larger radius would experience less resistance relative to their mass (in eq. (2), *i.e.* the parameter A is proportional to R_d^{-1}). Then, larger drops would seem to need smaller initial impact speeds to maintain the film prior to antibubble formation. However, we must not forget that the lubrication theory explains one aspect of antibubble formation: the formation of the air film. The pinching phenomenon is the other final determinant in whether the antibubble formation is successful. We will observe below that larger drops pinch off much slower than smaller drops because the time of pinch-off t_c is proportional to the radius of the cavity R_0, which is largely influenced by the initial aperture radius r_a. This slower pinching time is likely due to a greater volume of air trapped in the air film for larger drops [15]. Therefore, these observations may explain why in most of our experiments (*e.g.* 2 out of the 3 independent experiments reported in fig. 3) h_{opt} is positively correlated with r_a.

Pinching. We next consider the breakup of the liquid-air cavity that is formed upon impact of a drop with the surface. After formation of a cylindrical liquid column, which is surrounded by an annular film of air (fig. 1), we observe a pinching phenomenon that forms the final antibubble. The dynamics of the collapsing cylindrical column is reminiscent of the pinching of an inviscid fluid drop [16], as well as the collapse of a nearly cylindrical void following the impact of a solid with soft sand [17]; see also [18]. We now show that our data is most consistent with the capillary-driven pinching phenomena [16].

Using MATLAB image analysis software, we tracked the smallest radius of the pinch R until a singularity occurs. Because the actual pinching does not occur immediately, we define R_0 as when the drop has fully elongated, right before the continuous decrease in R begins to occur (fig. 1, frame d). The vertical scanning range for the software is determined manually to reduce errors (usually 0.5 mm below the free surface to a location that marks half of the elongated length), and values $R < 0.05$ are below our measurement threshold.

A Rayleigh-type collapse is observed for breakup of the liquid cavity. From the data we identified the time of collapse t_c (fig. 6a), and then with the functional form where the minimum radius is $R(t) \sim (t_c - t)^\alpha$, we extracted the exponent α by fitting the early-time data (since imaging errors increase for $t_c \approx t$). Representative data from two experiments are shown in fig. 6b, and have correlation coefficients 0.97 (squares) and 0.92 (triangles). The values of α extracted from the data are shown

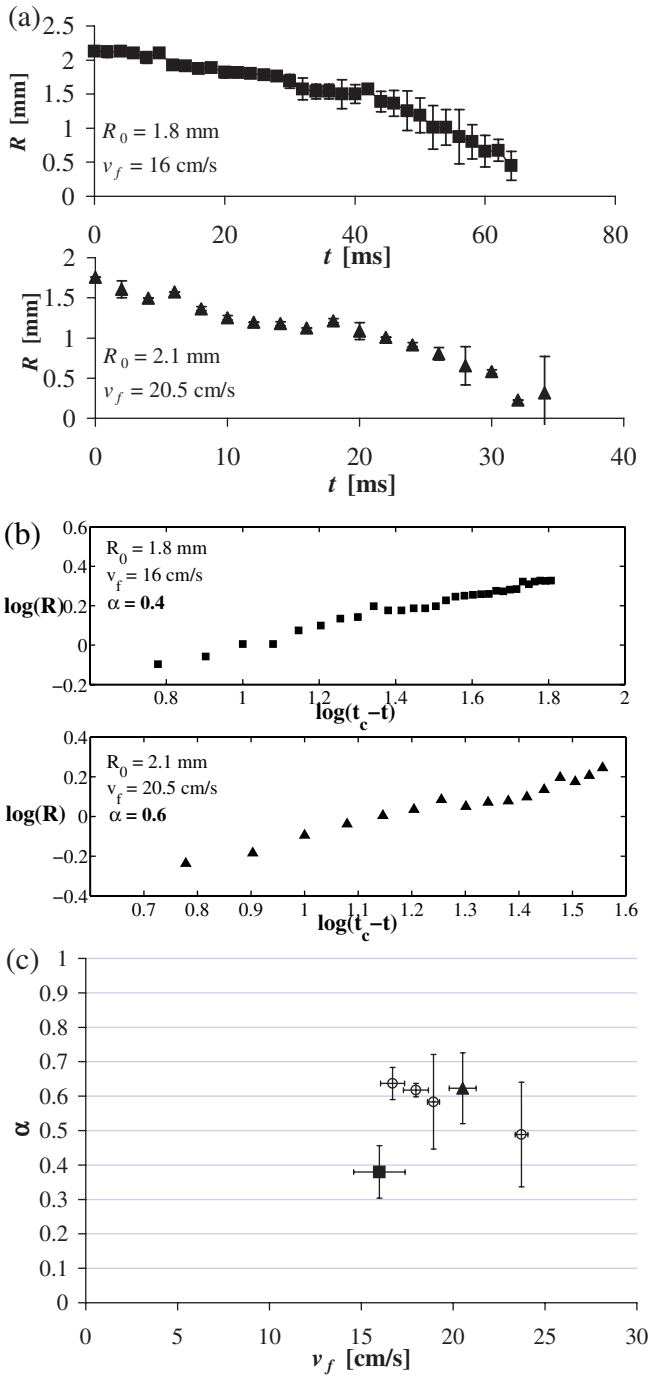

Fig. 6: Rate of pinching (exponent α) during the formation of antibubbles. (a) Plot of the radius of the pinch R *vs.* t under two conditions: $R_0 = 1.8$ mm, $v_f = 16$ cm/s (squares) and $R_0 = 2.1$ mm, $v_f = 20.5$ cm/s (triangles). Here v_f is the measured final impact speed on the surface. Error bars represent mean ± standard deviation. (b) The log-log plot of (a) to extract α. (c) Since $\alpha \approx 0.6$–0.7, most data support $R(t) \sim (t_c - t)^{2/3}$, where t_c is the time for collapse. The data in (a,b) are represented as filled points.

in fig. 6c and the majority cluster near 0.6–0.7. Therefore, we consider the dynamics to be driven by surface tension, in which case, neglecting the impact speed, the

radial evolution of a collapsing cavity is expected to follow [16] $R(t) \sim \left(\gamma(t_c - t)^2/\rho\right)^{1/3}$ and further we expect $t_c \approx \left(\rho R_0^3/\gamma\right)^{1/2}$. For drops having $R_0 \approx 2\,\mathrm{mm}$, this result predicts $t_c \approx 60\,\mathrm{ms}$, which is the order of magnitude of the measurements. We cannot rule out the role of gravity in driving the column collapse since $\left(\gamma/(\rho v_0^2 R_0)\right)^{1/2} = O(1)$. We originally consider the data from the view point of the irrotational, gravitationally driven collapse of a cylindrical column of fluid [17,18], but such models predict $\alpha = 1/2$, which is further from the majority of our data (fig. 6), and also show pinching substantially below the free surface, while in our experiments pinching occurs within 1–3 mm of the free surface (fig. 1). The data for $\alpha = 0.38$ (squares) is puzzling since it satisfies neither of the two theories; however, perhaps because of the low impact velocity, this elongated drop beneath the surface undergoes substantial reduction in its vertical length before the pinching is completed (larger drops tend to rise faster due to buoyancy which competes with the pinching dynamics), and the complicated dynamics do not fit a simple theory.

Therefore, our results can be interpreted thus: inertia of the liquid column along with viscous thinning of the air film mostly determines whether or not formation of an air film formation is successful, while surface tension usually drives the pinching of the liquid column, which actually seals and forms the antibubble. Previous papers have attributed antibubble formation to Rayleigh-Plateau capillary instability after observing a jet stream breaking up into individual antibubbles [10]. We believe that our results provide the first quantitative evidence that antibubble formation is indeed due to a capillary-driven pinching.

Conclusions. – At this time we know of no immediate applications for antibubbles and research in this field is limited, which may be due do the lack of consistency in the formation of these usually short-lived objects. Indeed, several significant advancements in the understanding of antibubbles only came after 2002 [8]. Nevertheless, here we have reported optimal conditions for making antibubbles in aqueous solutions, which may serve to facilitate other studies. For example, it may be possible to take advantage of the thin films that are easily created from antibubbles, which is especially promising since liquid-air interfaces may be used for biological or chemical reactions.

* * *

We thank the Harvard MRSEC (DMR-0213805) for partial support of this research. L. Courbin, E. Dressaire, B. Ristenpart and M. Sullivan are thanked for experimental suggestions and helpful conversations.

REFERENCES

[1] Frohn A. and Roth N., *Dynamics of Droplets* (Springer-Verlag, New York) 2000, pp. 245–260.
[2] Reyssat É., Chevy F., Biance A.-L., Petitjean L. and Quéré D., *Europhys. Lett.*, **80** (2007) 34005.
[3] Weiss P., *Sci. News*, **165** (2004) 311.
[4] Galvin K. P., Pratten S. J., Evans G. M. and Biggs S., *Langmuir*, **22** (2006) 522.
[5] Tufaile A. and Sartorelli J. C., *Phys. Rev. E*, **66** (2002) 056204.
[6] Hughes W. and Hughes A. R., *Nature*, **129** (1932).
[7] Strong C. L., *Sci. Am.*, **230** (1974) 116.
[8] Dorbolo S. and Vandewalle N., cond-mat/0305126 (2003).
[9] Dorbolo S., Reyssat E., Vandewalle N. and Quéré D., *Europhys. Lett*, **69** (2005) 966.
[10] Dorbolo S., Caps H. and Vandewalle N., *New J. Phys.*, **5** (2003) 161.
[11] Ioannou D., Huda W. and Laine A. F., *Image Vision Comput.*, **17** (1999) 15.
[12] Couder Y., Fort E., Gautier C.-H. and Boudaoud A., *Phys. Rev. Lett.*, **94** (2005) 177801.
[13] Dell'Aversana P. and Neitzel G. P., *Exp. Fluids*, **36** (2004) 299.
[14] Amarouchene Y., Cristobal G. and Kellay H., *Phys. Rev. Lett.*, **87** (2001) 206104.
[15] Kim P. G. and Vogel J., *Colloids Surf. A: Physicochem. Eng. Aspects*, **289** (2006) 237.
[16] Day D. F., Hinch E. J. and Lister J. R., *Phys. Rev. Lett.*, **80** (1998) 704.
[17] Lohse D., Bergmann R., Mikkelsen R., Zeilstra C., van der Meer D., Versluis M., van der Weele K., van der Hoef M. and Kuipers H., *Phys. Rev. Lett.*, **93** (2004) 198003.
[18] Duclaux V., Caille F., Duez C., Ybert C., Bocquet L. and Clanet C., *J. Fluid Mech.*, **591** (2007) 1.